Master in Oceanography

Facultad de Ciencias Básicas

Universidad de Las Palmas de Gran Canaria

Simulations of glacial/interglacial cycles with simple box-models. The ocean CO_2 source during deglaciations

Carmen Herrero i Navarro

Contents

Abstract

Paillard and Parrenin [2004] model has been modified to obtain a closer fit to $\delta^{18}O$ and CO_2 time-series for the last 800 kyr. Some sub-models have been developed, finding an improvement in performance if CO_2 sensitivity to I_{65} insolation is eliminated, and if different response times are assumed for both absorption/emission of CO_2 and for ablation/accumulation of ice. Correlations between simulated and experimental time-series have increased from 0.64 and 0.61 (for ice volume and CO_2) to 0.89 and 0.81, respectively.

It has been found that the model is almost insensitive to late Austral summer insolation (60ºS, 21st February) which leads to some conceptual changes, characterized in the Local Model with Double Stratification (LMDS). In LMDS, local proxies for Antarctic temperature have been used and stratification has been described to operate in two different ways: locally via the extent of Antarctic ice sheet and local temperature; and globally through global ice volume, V (which is strongly correlated to temperature changes in Northern Hemisphere), making a interconnection between oceanic pulse of CO_2 in Southern Ocean (SO) and Northern Hemisphere (NH).

According to this model, terminations are produced by I_{65} amplification, through $CO_2 - T$ and $T - CO_2$ feedback, in synergy with an extra CO_2 contribution coming from the deep ocean. This CO_2 pulse may be controlled by variations in the deep water formation rate in the Antarctic shelf, which is strongly dependent on ice volume and sea ice extent, being thus consistent with either a teleconnection mechanism via North Atlantic Deep Water upwelled in the SO (mechanism suggested by *Gildor and Tziperman* [2001]), or with sea-ice extent controlled by a local temperature (as suggested by *Paillard and Parrenin* [2004]).

Resumen

El modelo de *Paillard and Parrenin* [2004] ha sido modificado para obtener un mayor ajuste de las series experimentales de $\delta^{18}O$ y CO_2 para los últimos 800 kyr. Se han desarrollado varios sub-modelos, encontrando una mejora en los ajustes si la sensibilidad del CO_2 a la insolación I_{65} es eliminada y si se considera distintos tiempos de respuesta para la absorción/emisión de CO_2 y para la ablación/acumulación de hielo. Las correlaciones entre las series simuladas y experimentales han aumentado de 0.64 y 0.61 (volumen de hielo global y CO_2) a 0.89 y 0.81, respectivamente.

Se ha encontrado que el modelo es prácticamente insensible a la insolación Austral tardía (60ºS, 21 de Febrero) lo que lleva a ciertos cambios conceptuales, caracterizados en el Modelo Local con Doble Estratificación (LMDS). En LMDS, se han utilizado indicadores locales para la temperatura Antártica y la estratificación ha sido descrita para operar en dos sentidos: localmente mediante la extensión de capa de hielo Antártica y la temperatura local; y globalmente, mediante el volumen global de hielo, V (el cual está fuertemente correlacionado con variaciones de la temperatura en el Hemisferio Norte), dando lugar por tanto a una interconexión entre los pulsos oceánicos de CO_2 en el Océano Austral y el Hemisferio Norte.

De acuerdo con este modelo, las terminaciones están producidas por una amplificación de I_{65} mediante el feedback $CO_2 - T$ y $T - CO_2$, en sinergia con una contribución extra de CO_2 proveniente del océano profundo. Este pulso de CO_2 podría estar controlado por variaciones en la tasa de formación de aguas profundas en la plataforma Antártica, la cual es altamente dependiente del volumen de hielo y la extensión de hielo marino, siendo por tanto consistente tanto con un mecanismo de teleconexión mediante la North Atlantic Deep Water aflorada en el Océano Austral (mecanismo sugerido por *Gildor and Tziperman* [2001]), o con la capa de hielo marino controlada por la temperatura local (tal y como se sugiere en *Paillard and Parrenin* [2004]).

1 Introduction

Variations of glacial-interglacials states during the Quaternary are ultimately caused by changes in parameters of the Earth's orbit (*Hays et al.* [1976]) but other physical mechanisms must be involved and by now, they remain mostly unknown. Specifically, the role and mechanisms which involved an increase of atmospheric CO_2 during glacial-interglacial change are not entirely clear, although some exchange mechanisms involving the biological or the physical "carbon pumps" have been proposed to explain it (*Skinner* [2009]):

1. those involving an increase in the export rate of organic carbon to the deep ocean, either via increased nutrient availability at low latitudes or via increased efficiency of nutrient usage at high latitudes (*Broecker* [1982]; *Knox and McElroy* [1984]; *Kohfeld et al.* [2005])

2. those involving a reduction in the "ventilation" of water exported to the deep Southern Ocean (SO) (*Toggweiler and Sarmiento* [1985]; *Watson and Garabato* [2006])

3. those involving changes in ocean chemistry and "carbonate compensation", possibly promoted by changes in the ratio of organic carbon and carbonate fluxes to the deep sea (*Archer and Maier-Reimer* [1994]).

Each of this conceptual models has problems explaining the variation in glacial-interglacial CO_2 by itself, which probably suggest that none has operated in complete isolation (*Archer et al.* [2000]; *Sigman and Boyle* [2000]). What seems to be fundamental to explain CO_2 changes during glacial-interglacial states is the balance between biological sink of exported carbon from the surface-ocean and the returned carbon from deep circulation via physical mechanisms.

Regarding this physical pump, four main mechanisms have been identified which could modify its efficiency in glacial and interglacial times:

(a) Changes in the surface-to-deep mixing rate efficiency (*Toggweiler* [1999]; *Gildor and Tziperman* [2001]) and deep ocean stratification (*Paillard and Parrenin* [2004]). This mechanism is supported by proxies of temperature and salinity of deep water in the last glacial maximum (LGM) (*Adkins et al.* [2002]), which suggest that the density anomaly between Antarctic Bottom Waters (AABW) and intermediate waters was three times larger in the LGM than it is today. Therefore, if the rate of vertical mixing is inversely proportional to the density difference, the change in stratification of the deep ocean in glacial periods should be able to explain a fraction of the reduction of CO_2 input to the atmosphere due to diapycnal mixing variation in deep waters (*Watson and Garabato* [2006]).

(b) Sequestration of CO_2 in deep waters with a standing volume that increases during glacial climates. Southern-sourced deep water was found in the deep North Atlantic up to a water depth of 2.5 km in the past glacial age (*Curry and Oppo* [2005]) which suggests an increase of southern-sourced water. *Skinner* [2009] calculates that, for glacial ages, a rising in the level of AABW and Low Circumpolar Deep Water, LCDW (having average total dissolved CO_2 concentrations of 2280 µmol kg^{-1}) from 20 million km^3 to 70 million km^3 (a 4-fold increase) at the expense of NADW (having 2180 µmol kg^{-1}) would produce an oceanic gain of 63 Gt of carbon. If all this carbon comes from the atmosphere, then atmospheric pCO_2 would have to drop by 30 ppm, given 1 ppm change per 2.12 Gt carbon removed from the atmosphere. This is equivalent to 34% of the CO_2 increase observed after glacial-interglacial change.

(c) Switching off/on of the Antarctic upwelling at Drake Passage latitudes in cold/warm conditions (*Toggweiler et al.* [2006]). Any process producing a (global or southern) tropospheric warming would imply poleward-shifted westerlies, possibly through increased evaporation. This would produce stronger wind-stress work at the Drake Passage latitudes and stronger upwelling of deep water at the SO divergence.

(d) Extended ice sea in the SO produces a “capping” effect on the CO_2 release to the atmosphere during winters (*Keeling and Stephens* [2001]) and a retardation of the overturning rate in the SO due to sea ice control on the residual circulation (*Watson and Garabato* [2006]; *Fischer et al.* [2010]).

In all of the mechanisms above, an increased CO_2 release is expected during the change between glacial-interglacial periods, and it is expected to take place mainly in the SO. Interestingly, recent proxies obtained for the temperature at Antarctica show a strong correlation between temperature and CO_2 concentrations (*Siegenthaler et al.* [2005]; *Fischer et al.* [2010]). On the other hand, recent interpretations (*Paillard* [2010]) of empirical data (*Bard et al.* [1996]; *Monnin et al.* [2001]) suggest that the atmospheric CO_2 concentration increased for several millennial before the melting of the northern hemisphere ice sheets. Both pieces of evidence support the hypothesis that some of the mechanisms mentioned above, taking place essentially in the SO, could be behind the increase of CO_2 needed to produce glacial-interglacial change.

Some simple box models have been proposed to explain this so-commented glacial-interglacial cycles. Some of them, as *Pelegrí* [2008] and *Pelegrí et al.* [2011] take into account changes in overturning rate and biological exportation of CO_2, reproducing approximately sawtooth-like oscillation of last four glacial cycles but in which physical triggers of glacial-interglacial states remain unexplained. More complex models as *Ganopolski et al.* [2010] have shown that Earth system models of intermediate complexity (EMICs) as CLIMBER-2 are able to reproduce the major aspects of glacial cycles under orbital and greenhouse forcing rather realistically. However, the CO_2 forcing has to be introduced independently of the orbital forcing.

Paillard and Parrenin [2004] also proposed a simple box-model (PP04 model hereafter) but taking into account the mechanism of dense water formation in the Southern Ocean. In this model the Antarctic ice-sheet extent is proposed as a new mechanism able to link climatic and CO_2 glacial-interglacial changes. The clue of their results is the identification of ocean-CO_2 switch based on the vertical density structure of the deep ocean as the largest non linearity of the system. In spite of its simplicity, this model is the first one to accurately reproduce pace and termination times of all glacial-interglacial cycles during Quaternary, as well as the whole set of maxima and minima of the $\delta^{18}O$ (*Lisiecki and Raymo* [2005]) oscillations observed in the past 5 million years. This may be a sign of the crucial role played by the stratification and Southern Ocean CO_2 pulse in the onset of glacial-interglacial change.

García-Olivares and Herrero [2011] (shown in Appendix) generalizes and calibrates PP04 model to the $\delta^{18}O$ and CO_2 time-series available for the last 800 kyr (*Lisiecki and Raymo* [2005]; *Monnin et al.* [2001]; *Petit et al.* [1999]; *Pepin et al.* [2001]; *Siegenthaler et al.* [2005]; *Luthi et al.* [2008]) with the aim of analyzing how different generalizations, such as export production or the strength of deep stratification, could affect some improvements at experimental fits. It was observed that the PP04 model performance can be improved if its CO_2 sensitivity to insolation is eliminated and if different response times were assumed both for absorption/emission of CO_2 and for ablation/accumulation of ice. We will refer to this model hereafter as 4τ (*Herrero et al.* [2010, 2011])

PP04 and specially 4τ model are fully explained, mathematically and dynamically, on following sections.

2 Methods

In this section are specified the different software and methods applied to obtain the results.

2.1 Insolation

To calculate insolation at different latitudes the software used was *Berger* [1978a], with a modified script made by *Olivella* [2009]

In this work, different insolation data have been used to cover time domain between -800 kyr and 0 yr (present time) with time steps of 100 yr. On one hand, insolation regarding one single day of the year at one specified latitude, this is Northern Hemisphere summer insolation (65ºN on 21st June) and late Austral summer insolation (60ºS on 21st February), both of which are calculated directly with Berger's software (*Figure 2.1.1*)

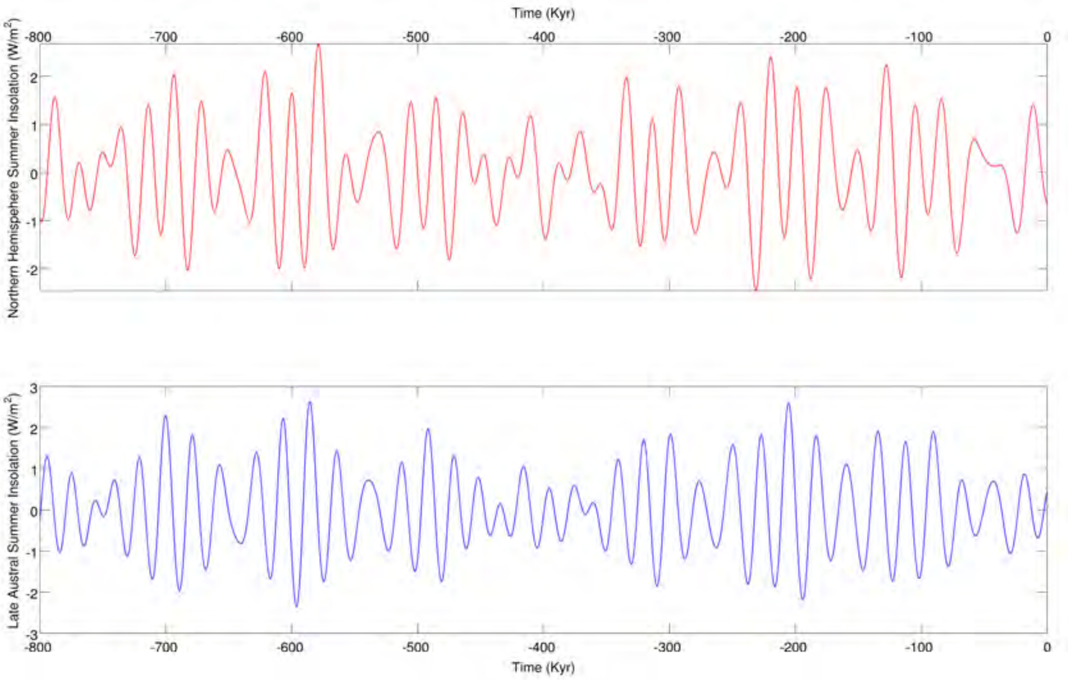

Figure 2.1.1: Northern Hemisphere summer insolation (top) and late Austral summer insolation (bottom).

On the other hand, we have calculated average insolation of Austral summer (shown in *Figure 2.1.2*), from 21st November to 21st March. To do so, two different files have been generated with Olivella's script: a file with monthly insolation of November and December for every year and another one with monthly insolation of January, February and March, also for every year. We do this because every Austral summer involves two different years, so, we have calculated Austral summer insolation for every year as the mean of November and December plus mean of January, February and March of the next year. The last year, corresponding at present time was calculated as mean of November and December of 0 yr plus mean of January, February and March of +100 yr.

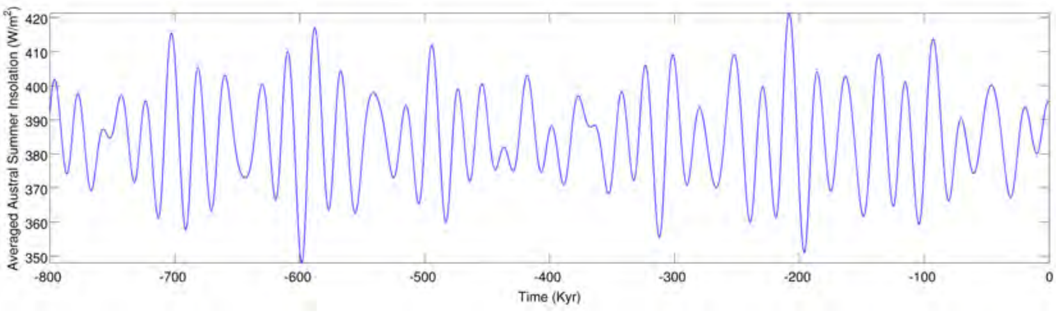

Figure 2.1.2: Averaged insolation of Austral summer.

Using this data, another insolation set has been generated, but instead of doing the mean for every summer, doing the integration of monthly insolation to get summed insolation for every Austral summer. As shown in *Figure 2.1.3*, all three cases have almost exactly the same shape.

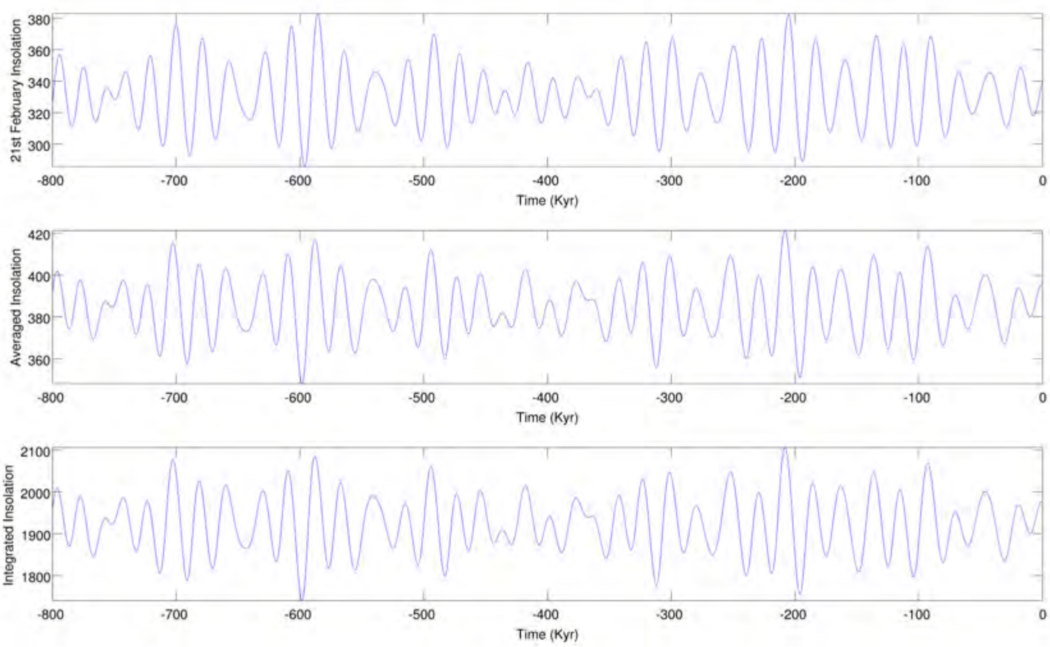

Figure 2.1.3: Comparison between late Austral summer insolation (top), averaged summer insolation (middle) and integrated summer insolation (bottom).

2.2 Optimizations

To perform optimizations of mathematical expressions, we have implemented a multiobjective genetic algorithm with the aim of maximize correlation between experimental and modeled data. This has been done with Global Optimization Toolbox from Matlab[1].

First of all, we must answer a key question: what exactly is a genetic algorithm?

According to *Charbonneau* [2002], genetic algorithms are, fundamentally, a class of search techniques that use simplified forms of the biological processes of selection/inheritance/variation.

This optimizers are based on natural selection, which states that individuals better adapted to their environment, i.e., for whatever reason better at obtaining food, avoiding becoming lunch, and finding/attracting/competing for mates, will, on average, leave behind more offspring than their less apt colleagues.

For natural selection to lead to evolution, two more essential ingredients are required:

1. inheritance: offspring must retain at least some of the features that made their parents fitter than average, otherwise evolution is effectively reset at every generation.

2. variability: at any given time individuals of varying fitnesses must coexist in the population, otherwise natural selection has nothing to operate on.

To better understand the mechanism, here we show a genetic optimization problem based in our model. One is given a model that depends on a set of parameters u (like 4τ), and a functional relation $f(u)$ that returns a measure of quality, or fitness, associated with the corresponding model (in our case, this function is the correlation between the modeled output and the experimental data). The optimization task usually consists in finding the "point" $u*$ in parameter space corresponding to the model that maximizes the fitness function $f(u)$ (in our case, we search in a parameter space of 15 or 16 coordinates). Define now a population as a set of N_p realizations of the parameters u.

A top-level view of a basic genetic algorithm is then as follows:

1. Randomly initialize population and evaluate fitness of its members (parents)

2. Breed selected members of current population to produce offspring (child) population (selection based on fitness)

3. Replace current population by offspring population

4. Evaluate fitness of new population members

5. Repeat steps (2) through (4) until the fittest member of the current population is deemed fit enough.

[1]Matlab is a software from MathWorks. Inc.

The crucial novelty lies with step 2: *Breeding*. It is in the course of breeding that information is passed and exchanged across population members through mechanisms as crossover (also called recombination) and mutation. As the name suggests, crossover is a process of taking more than one parent solutions and mix them to produce a child. In the mutation, some parents are randomly change to produce some variations in evolution (just as mutation works in natural environment).

This is how genetic algorithm works from a very simplified point of view. We have used this technique to set all 16 parameters (or 15, depending on the case) that form the model in order to find the combination that maximizes the correlation.

3 Models

3.1 PP04 model

Just as a quick reference, here is shown the basic structure of the model developed by *Paillard and Parrenin* [2004], which is formed by three variables: global ice volume, V; extent of Antarctic ice sheet, A; and atmospheric CO_2, C. All parameters are fully explained in 4τ model section. The mathematical expression to lately compare with other models follows.

$$\frac{dV}{dt} = \frac{(V_r - V)}{\tau_V} \tag{3.1.1}$$

$$\frac{dA}{dt} = \frac{(V - A)}{\tau_A} \tag{3.1.2}$$

$$\frac{dC}{dt} = \frac{(C_r - C)}{\tau_C} \tag{3.1.3}$$

$$V_r = -xC - yI_{65} + z \tag{3.1.4}$$

$$C_r = \alpha I_{65} - \beta V + \gamma H(F) + \delta \tag{3.1.5}$$

$$F = aV - bA - cI_{60} + d \tag{3.1.6}$$

An interesting result of PP04 model is how introducing a small drift $(d{+}kt)$ in oceanic parameter F over the last million years, the model is able to reproduce most glacial-interglacial cycles over this period, changing oscillations frequency from 23 to 41 kyr (around 3 Myr BP) and from 41 to 100 kyr (around 1 Myr BP). Shown in *Figure 3.1.1.*

The success of this model in correctly reproducing ice volume and atmospheric CO_2, all nine glacial-interglacial cycles for the Quaternary, as well as changes in oscillations frequency over the last millions years, indicates that the underlying physical mechanisms and specially the vertical density structure of the deep ocean could be essential to understand glacial-interglacial oscillations.

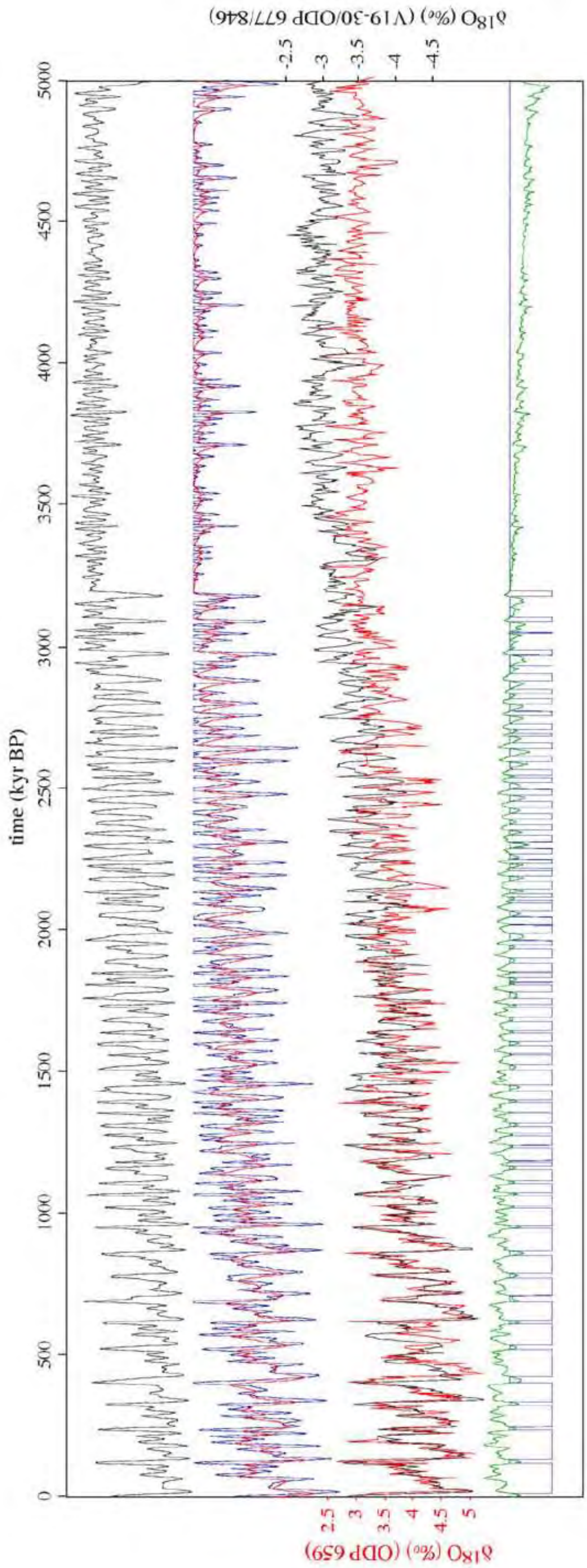

Figure 3.1.1: PP04 model results over the last 5 Myr (*Paillard and Parrenin* [2004])

3.2 4τ model

4τ model, as PP04 model, is formed by three dimensionless indexes: V, representing global ice volume and forced by Northern Hemisphere summer insolation (I_{65}) and atmospheric CO_2; the extent of Antarctic ice sheet, A, which is forced by sea level changes through V; and atmospheric CO_2, C, linked to global ice volume and deep-ocean CO_2 contribution, which depends as a Heaviside Function[1] on the "salty bottom water formation efficiency parameter", F.

Structure is the following:

$$\frac{dV}{dt} = \frac{(V_r - V)}{\tau_V} \tag{3.2.1}$$

$$\frac{dA}{dt} = \frac{(V - A)}{\tau_A} \tag{3.2.2}$$

$$\frac{dC}{dt} = \frac{(C_r - C)}{\tau_C} \tag{3.2.3}$$

$$V_r = -xC - yI_{65} + z \tag{3.2.4}$$

$$C_r = -\beta V + \gamma H(F) + \delta \tag{3.2.5}$$

$$F = aV - bA - cI_{60} + d \tag{3.2.6}$$

The principal variables V, A and C tend exponentially to a reference state V_r, V and C_r at characteristic times τ_V, τ_A and τ_C, respectively. V_r decreases when C increases, and when I_{65} is high. C_r increases when the oceanic pulse of CO_2 is *on*, and decreases when the ice volume increases. The β parameter represents the positive feedback between global ice volume and CO_2. The parameter δ can be interpreted as a CO_2 geophysical reference-level that is constant or dependent only on long-term tectonic activity. On the other hand, F parameter increases when the amount of global ice grows (through V) and decreases when continental shelf areas are reduced (through increased A) and when late Austral summer insolation I_{60} (60ºS, 21st February) increases.

Two different response times are used for the accumulation and absorption of CO_2: $\tau_C = \tau_{C1}$ for the periods where $C < C_r$ and $\tau_C = \tau_{C2}$ when $C > C_r$. Similarly, two different response times are used for accumulation and ablation of ice: $\tau_V = \tau_{V1}$ for periods when $V < V_r$ and $\tau_V = \tau_{V2}$ when $V > V_r$. Physically, two characteristic times for melting (τ_{V2}) and accumulation of ice (τ_{V1}) are justified because they are different processes; specifically, it is necessary that $\tau_{V1} > \tau_{V2}$, because melting is faster than accumulation.

[1]Heaviside Function: $H = 1$ if $F < 0; H = 0$ otherwise

However, two response times for emission (τ_{C2}) and absorption (τ_{C1}) of atmospheric CO_2 are harder to explain. *Archer et al.* [2009] reviewed literature on the carbon cycle and discussed some models, getting to the conclusion that it will take a timescale of 2 to 20 centuries for the ocean to absorb the surplus atmospheric CO_2, and even when the equilibrium would be reached, a substantial fraction (20-40%) of this CO_2 would remain in the atmosphere awaiting slower chemicals reactions. These results are apparently coherent with the situation proposed here, where $\tau_{C2} > \tau_{C1}$, but further investigation is needed to have a precise understanding of the long-term carbon cycle.

Daily insolation for the last 800 kyr is obtained from the *Berger* [1978b, a] software as it is shown in section 2. Insolation is normalized with its standard deviation to obtain I_{65} and I_{60}. No lower bound is imposed on the V, C and A variables. Note that all results of the model have been normalized by their standard deviation before plotting.

Parameter	PP04 Model	4τ Model with α	4τ Model without α
τ_{V1}	15000	13297.6	16342.12
τ_{V2}	-	2437.42	3641.46
τ_{C1}	5000	5353.01	12036.02
τ_{C2}	-	10503.07	19282.14
τ_A	12000	9424.83	6159.27
x	1.3	0.753	1.288
y	0.5	0.646	0.65
z	0.8	1.199	1.173
α	0.15	0.218	-
β	0.5	0.631	0.386
γ	0.7	2.312	1.922
δ	0.4	0.528	0.169
a	0.3	0.711	0.833
b	0.7	1.399	1.599
c	0.01	0.011	0.126
d	0.27	0.486	0.637
ρ_V	0.64	0.88	0.89
ρ_C	0.61	0.80	0.81

Table 3.1: Parameter values used in each model. ρ_V and ρ_C represent the correlation between experimental and modeled data for V and C respectively. In original *Paillard and Parrenin* [2004], γ parameter had a value of 0.5 due to a mistake. Noticed by Michael Crucifix and Didier Paillard in a later revision, the correct value is 0.7.

The original PP04 model includes direct forcing of the I_{65} insolation on the CO_2 response (α parameter on *Eq. 3.1.5*). The physical interpretation of this forcing is not clear, given that the CO_2 response to temperature is already included in the model. 4τ model has been run with both possibilities (including and not including α as a parameter), given that

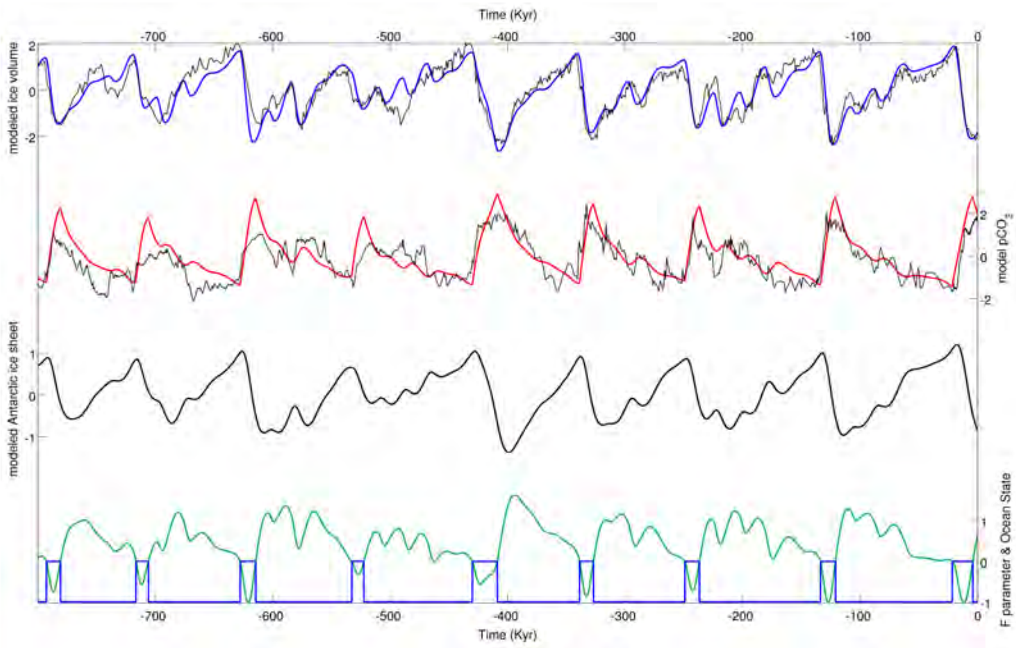

Figure 3.2.1: 4τ model with α over the last 800 kyr. Top, modeled ice volume (blue) and $\delta^{18}O$ experimental time-series obtained by *Lisiecki and Raymo* [2005] (black, thin line); below, simulated CO_2 levels (red) and experimental time-series obtained by *Luthi et al.* [2008] (black, thin line); below, modeled Antarctica area (black); and bottom, critical parameter F (green) and the state of the ocean (blue): glacial or interglacial.

the best fits were obtained when this forcing is zero (*Table 3.1*), hereafter when we will be referring to 4τ model it will be without α parameter.

It is interesting how α parameter is responsible of high-frequency oscillations in CO_2, making visually modeled and experimental curve seem more different, although the correlation obtained is slightly higher (*Figures 3.2.1* and *3.2.3*)

As can be observed in *Figures 3.2.2, 3.2.3* and *3.2.4*, 4τ model is much more like a saw-tooth oscillation, like experimental data, than PP04 model does. The C series presents a saw-shaped form also, which is produced by the feedback V-C (through β) in conjunction with the large value used for the parameter τ_{C2}. Is interesting how the introduction of two different response times, as well the suppression of α parameter affects the shape and high-frequency of the CO_2 oscillations. Both models have some problems simulating the maxima of 500 kyr BP, as well as terminations VII and VIII, which none of the models are able to reproduce shape nor timing.

In 4τ model, many details of the high-frequency oscillations of the experimental ice volume are better simulated than in PP04. The shape of the cycles I, III, IV and VII BP are also adequately simulated. However, it can be observed that both models have difficulty simulating the glacial cycle between 600 and 700 kyr BP, specially the timing of its termination, but 4τ model is able to predict accurately the timing of Terminations II and IV. This is probably a shared limitation of both model and $\delta^{18}O$ records. As has

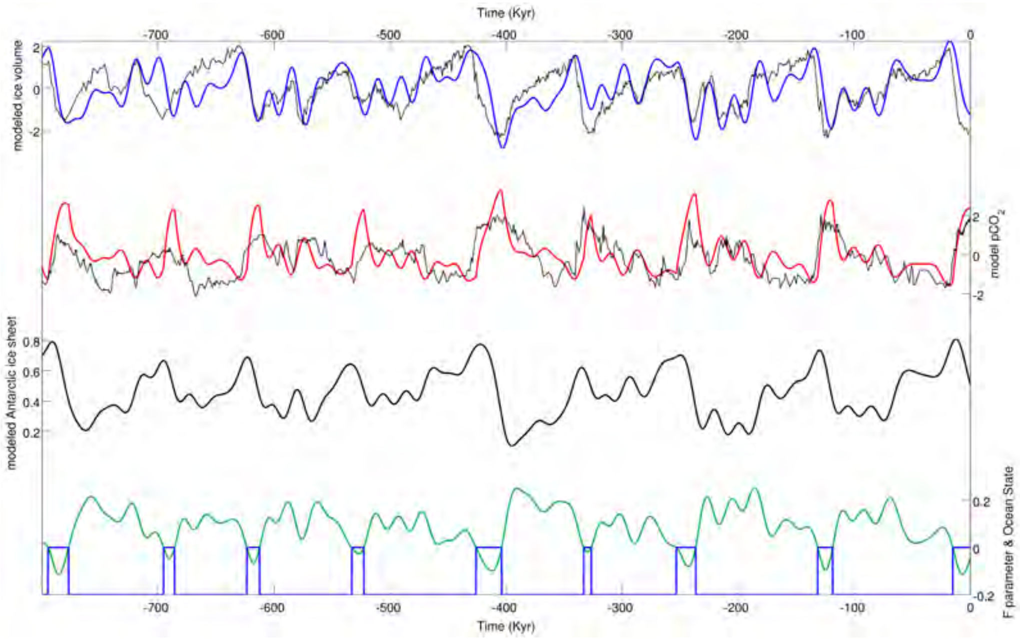

Figure 3.2.2: Model results for PP04 as shown in *Paillard and Parrenin* [2004]. Top, modeled ice volume (blue) and $\delta^{18}O$ experimental time-series obtained by *Lisiecki and Raymo* [2005] (black, thin line); below, simulated CO_2 levels (red) and experimental time-series obtained by *Luthi et al.* [2008] (black, thin line); below, modeled Antarctica area (black); and bottom, critical parameter F (green) and the state of the ocean (blue): glacial or interglacial (zero value).

been suggested by Paillard, almost all paleoclimatic records are, in some way, tuned to the astronomical forcing by using implicitly or explicitly a simple model of ice ages. In other words, it is not clear that the time scale of the data is better or worse than the time scale of the model (within, lets say, a quarter period of the fastest forcing, the precession, i.e. ± 6 kyr). This is particularly true for the timing of terminations which may not be constant versus the forcing (see e.g. *Parrenin and Paillard* [2003]). For this reason, a "better fit" of the timing of terminations of the $\delta^{18}O$ data may not be an improvement, since the data are not necessarily very accurate and may be biased by assumptions that are too simple.

As shown, in *Table 3.1*, parameter c, which relates the efficiency of dense water formation with late Austral summer insolation, is relatively small. Curiously, an almost identical optimum can be found with a set of parameters that does not use the I_{60} forcing (i.e. $c = 0$).

This result can be interpreted in three alternative ways:

i. I_{60} is not a good proxy for Southern Ocean temperature;

ii. The formation of dense water and/or CO_2 release in the Southern Ocean is not controlled by local temperature;

iii. The release of CO_2 in the SO is not controlled by deep water density, and the function $F(V, A)$ in our models represents a different process.

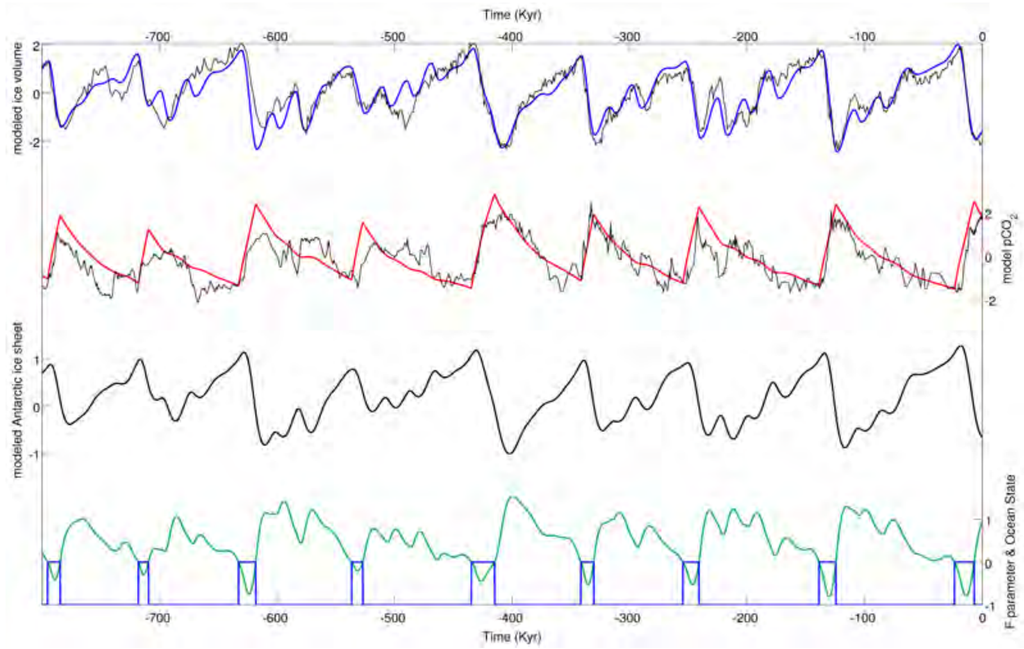

Figure 3.2.3: 4τ model with α=0. Top, modeled ice volume (blue) and $\delta^{18}O$ experimental time-series obtained by *Lisiecki and Raymo* [2005] (black, thin line); below, simulated CO_2 levels (red) and experimental time-series obtained by *Luthi et al.* [2008] (black, thin line); below, modeled Antarctica area (black); and bottom, critical parameter F (green) and the state of the ocean (blue): glacial or interglacial (zero value).

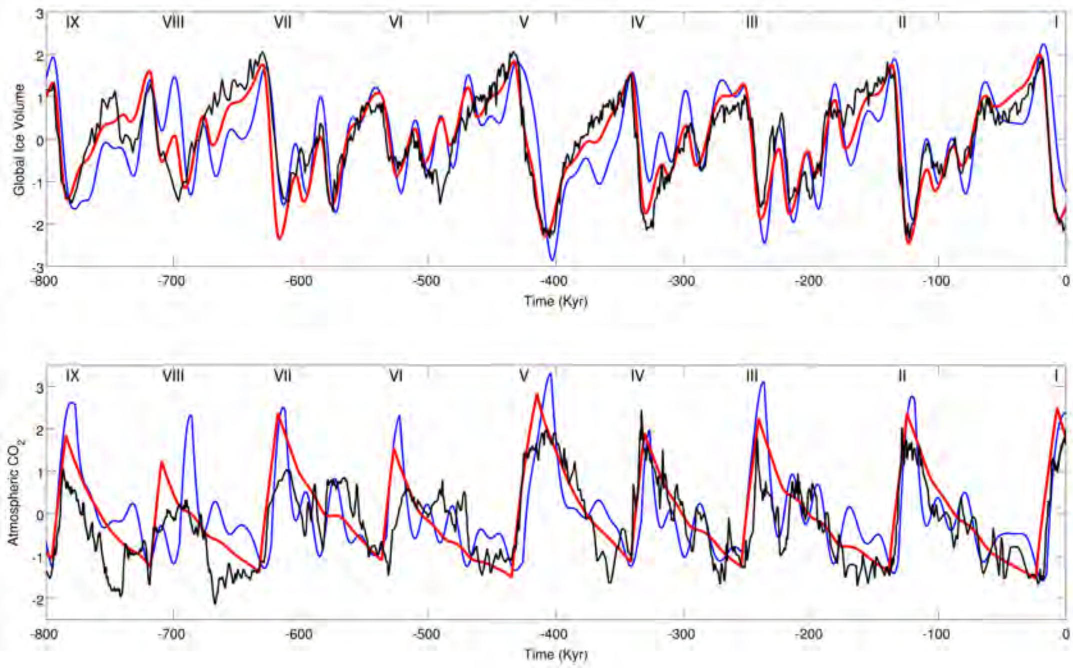

Figure 3.2.4: Comparison between Global ice volume (top) predicted by PP04 (blue), 4τ (red) and $\delta^{18}O$ experimental time-series obtained by *Lisiecki and Raymo* [2005] (black) and CO_2 (bottom) predicted by PP04 (blue), 4τ (red) and experimental time-series obtained by *Luthi et al.* [2008] (black).

To explore the third possibility, we conjectured that $F(V, A, I_{60})$ may be a proxy for the change of CO_2 release due to variations in upwelling intensity at Drake Passage latitudes. Upwelling intensity should increase when atmospheric convective cells intensify due to increased global and local evaporation; therefore, in our model, it should decrease with V and rise with I_{60}. If this conjecture were correct, then *Equation 3.2.2* would be unnecessary, and the system of *Equations 3.2.1, 3.2.3, 3.2.4* and *3.2.5* may also have a good fit using a different set of parameter values. Consequently, we explored the new equations system for a wider region of the parameter space. However, no fit was found that could reproduce the pace of the last glacial cycles.

Another possible interpretation is that $F(V, A, I_{60})$ could be a proxy for a rate of emission of CO_2 that is controlled directly by sea ice area, A, and local temperature. Local temperature could be controlled by global temperature more strongly than by I_{60}. One possible mechanism able to produce this effect was proposed by *Gildor and Tziperman* [2001]: stratification in the SO is composed of cold, fresh and therefore light water above warm, salty and therefore dense water. Glacial conditions in the northern hemisphere cool the North Atlantic Deep Water (NADW) and, consequently, via the southward flow and upwelling of NADW, lower the deep temperature in the SO. Because of permanent ice cover over Antarctica, surface ocean temperature in the SO near Antarctica is close to freezing point during the entire glacial cycle, so that it cannot cool very much even during glacial conditions. Glacial conditions, therefore, increase the density of deep SO water but not of surface SO water and this strengthens the vertical stratification there. As a result, vertical mixing in the SO is expected to be reduced. This mechanism implies that temperature changes in the northern hemisphere (strongly correlated with global ice volume V) lead to CO_2 changes in the southern hemisphere. To test if A is sensitive to I_{60}, *Equation 3.2.2* of the model was modified in the following way:

$$\frac{dA}{dt} = \frac{(V - A - cI_{60})}{\tau_A} \tag{3.2.7}$$

However, the best fits obtained after this change did not improve upon those obtained by 4τ model.

These results are consistent with the following conclusions: An A variable, probably related to sea ice extent that follows the evolution of V with a delay of 5 to 15 kyr seems necessary to obtain good fits. CO_2 release to atmosphere in the SO may be controlled either by density of deep water or by sea ice extent or both. However, none of the two mechanisms seems to be sensitive to I_{60} insolation. Either some of these mechanisms are not sensitive to SO temperature, which is difficult to conceive, or I_{60} is not a good proxy for SO temperature.

Huybers and Denton [2008] have pointed out an important fact that had passed unperceived and that could be coherent with these conclusions: Antarctic summer duration is highly correlated with I_{65} insolation. In addition, it is plausible that Antarctic climate remains in near radiative equilibrium with local heat accumulation, which is controlled by

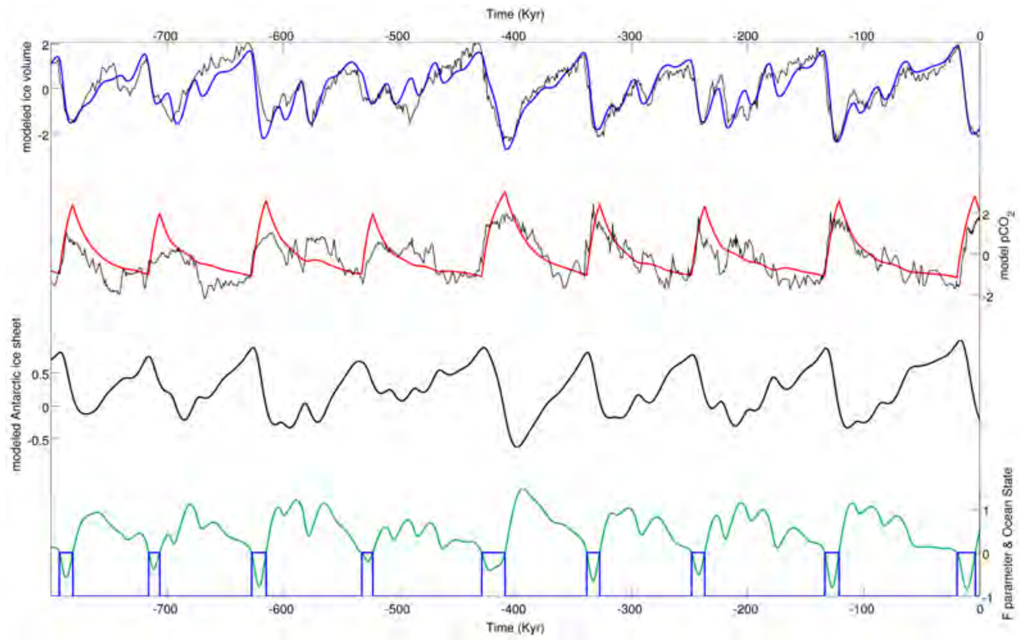

Figure 3.2.5: 4τ model with α=0 and I_{60}^{AV}. Top, modeled ice volume (blue); below, simulated CO_2 levels (red); modeled Antarctica area (black); and bottom, critical parameter F (green) and the state of the ocean (blue): glacial or interglacial (zero value).

summertime duration. In contrast, northern changes are mediated through the response of the northern ice sheets, which are much more sensitive to insolation at the solstice (I_{65}) than to summertime duration. Thus, SO temperature could be a crucial variable that controls either the southern sea ice or the density of deep water or both; but this southern temperature does not need to be controlled via teleconnection with the north. It may responds directly to local astronomical forcing different to I_{60}. Some simulations have been done with other proxies for I_{60}, for instance using integrated insolation of Austral Summer (I_{60}^{IN}) or averaged insolation of Austral Summer (I_{60}^{AV}), in order to have some light on the subject.

3.2.1 Another proxy for I_{60}

As is shown in *Figure 2.1.3*, three different insolation sets have been generated, all of which have almost exact shapes. It is said above and according to *Huybers and Denton* [2008], that the duration of Southern Hemisphere summer is what probably controls Antarctic climate. In spite of having generated two new sets of insolation (I_{60}^{IN} and I_{60}^{AV}), and despite having been used both in 4τ model, here are shown the results using I_{60}^{AV} instead of I_{60}, since the similarity between sets of insolation (I_{60}^{IN} or I_{60}^{AV}) provides no differences when running the model.

It can be noticed that there is no real difference between using I_{60}^{AV} or I_{60} (*Figure 3.2.5*), which was actually expected due to both sets of insolation have almost same shape. The conclusion to be drawn have been mentioned before: I_{60} clearly is not a good proxy for

Southern Ocean temperature, for which is necessary more investigation, that will lead us to change some concepts of the model. In line with *Gildor and Tziperman* [2001], other expressions for local temperature have been searched for.

On the other hand, it will be interesting explore with further research how a set of summertime, instead of late Austral summer insolation, affects the model, as *Huybers and Denton* [2008] had proposed, being this the subject of future work.

4 Results

Some proxies have been proposed to replace I_{60}, since it has been demonstrated that it is not a good proxy for Southern Ocean temperature. Here we show two different models both of which are based on local proxies.

4.1 LMSS model

In this Local Model with Simple Stratification (LMSS hereafter) the insolation in the Southern Hemisphere (SH) has been substituted for modeled variable C. Since atmospheric CO_2 can be considered as temperature proxy (depending on location, temperature often looks like CO_2, for instance in the Antarctic deuterium record) and due to oceanic CO_2 pulse takes place in SO, variable C can be considered as a valid proxy of local temperature in SH.

This model proposed here, takes into account a simple mechanism of stratification through the extent of Antarctic ice sheet and local temperature, C. Basically, the "salty bottom water formation efficiency parameter", F, is only controlled by local mechanisms in the SO, and so does oceanic pulse of CO_2 which could be responsible of changes in glacial-interglacial states.

The mathematical expression follows.

$$\frac{dV}{dt} = \frac{(V_r - V)}{\tau_V} \tag{4.1.1}$$

$$\frac{dA}{dt} = \frac{(-C - A)}{\tau_A} \tag{4.1.2}$$

$$\frac{dC}{dt} = \frac{(C_r - C)}{\tau_C} \tag{4.1.3}$$

$$V_r = -xC - yI_{65} + z \tag{4.1.4}$$

$$C_r = -\beta V + \gamma H(F) + \delta \tag{4.1.5}$$

$$F = -bA - cC + d \tag{4.1.6}$$

Here, the Antarctic ice sheet reference, represented before by V, has been changed to

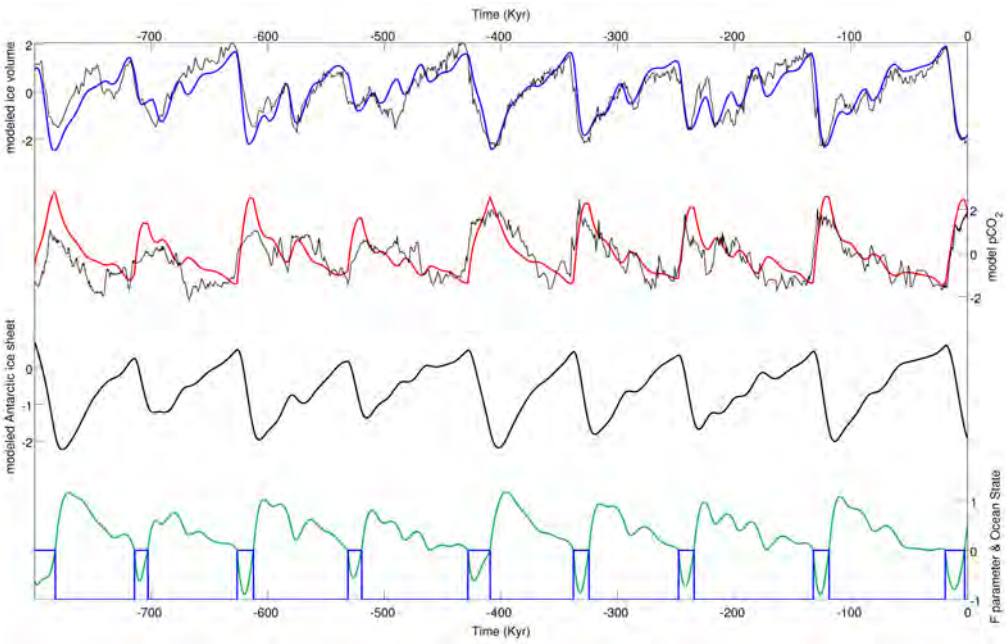

Figure 4.1.1: LMSS model over the last 800 kyr. Top, modeled ice volume (blue); below, simulated CO_2 levels (red); below, modeled Antarctica area (black); and bottom, critical parameter F (green) and the state of the ocean (blue): glacial or interglacial (zero value).

$-C$ in *Equation 4.1.2* and similarly, insolation of Southern Hemisphere has been replaced by C in *Equation 4.1.6*, as well as the dependency $F(V)$ has been removed.

4.2 LMDS model

Another possibility, following previous line, is to consider stratification dependent on local and global variables. Thus, a Local Model with Double Stratification (LMDS hereafter) has been developed, in which structure is virtually identical to LMSS except that stratification operates in two different ways: locally via the extent of Antarctic ice sheet and local temperature; and globally through global ice volume, V (which is strongly correlated to temperature changes in Northern Hemisphere), making a interconnection between oceanic pulse of CO_2 and Northern Hemisphere (NH).

Mathematical expression is the following.

$$\frac{dV}{dt} = \frac{(V_r - V)}{\tau_V} \tag{4.2.1}$$

$$\frac{dA}{dt} = \frac{(-C - A)}{\tau_A} \tag{4.2.2}$$

$$\frac{dC}{dt} = \frac{(C_r - C)}{\tau_C} \tag{4.2.3}$$

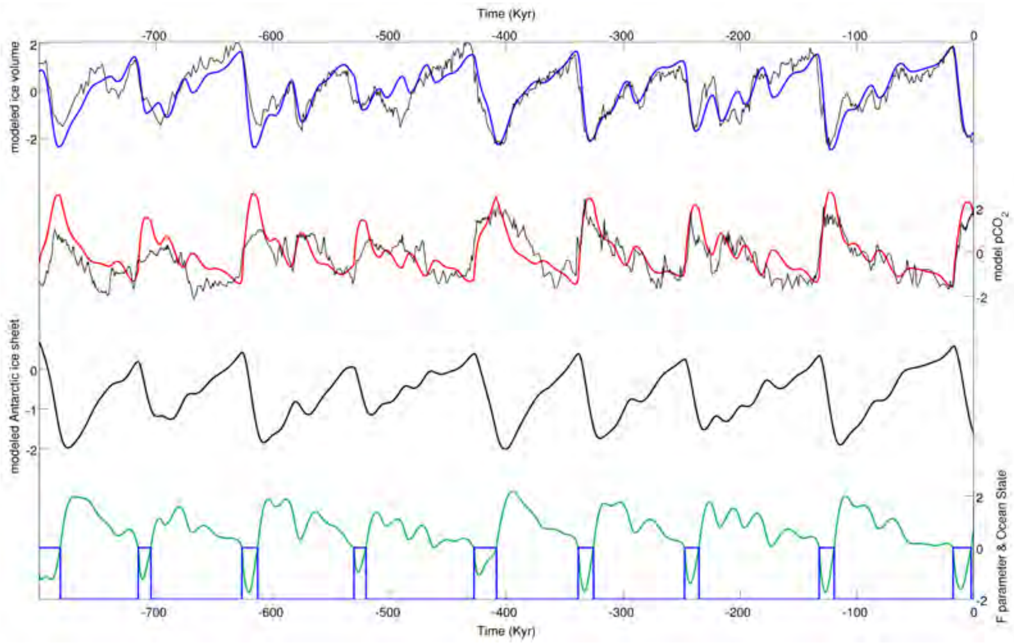

Figure 4.2.1: LMDS model over the last 800 kyr. Top, modeled ice volume (blue); below, simulated CO_2 levels (red); below, modeled Antarctica area (black); and bottom, critical parameter F (green) and the state of the ocean (blue): glacial or interglacial (zero value).

$$V_r = -xC - yI_{65} + z \tag{4.2.4}$$

$$C_r = -\beta V + \gamma H(F) + \delta \tag{4.2.5}$$

$$F = aV - bA - cC + d \tag{4.2.6}$$

Note that difference with LMSS remains in F parameter, where the dependency with V has been added.

As shown in *Figures 4.1.1* and *4.2.1*, both models are extremely similar; in fact, LMSS gives slightly better results than LMDS, but this last one has more physical consistence, due to the agreement with recent interpretations (*Paillard* [2010]) of empirical data (*Bard et al.* [1996]; *Monnin et al.* [2001]) which suggest that the atmospheric CO_2 concentration increased for several millennial before the melting of the northern hemisphere ice sheets, being this impossible to explain with LMSS.

They both reproduce more high frequency than 4τ model does in CO_2 curve, specially LMDS, and it is able to better reproduce the timing of almost all cycles, except IX, where it has problems reproducing shape and time. In LMDS, pace and timing of ice volume for

Parameter	LMSS Model	LMDS Model
τ_{V1}	11101.9	11392.31
τ_{V2}	2348.89	3118.3
τ_{C1}	3350.01	1876.51
τ_{C2}	8408.9	8218.61
τ_A	10388.85	14596.74
x	0.778	0.547
y	0.53	0.341
z	0.837	0.878
α	0.285	0.488
β	0.677	0.839
γ	1.933	1.902
δ	0.135	0.3
a	0.813	0.081
b	0.918	1.577
c	0.514	0.718
d	0.073	0.064
ρ_V	0.87	0.86
ρ_C	0.75	0.74

Table 4.1: Parameter values used in each model. ρ_V and ρ_C represent the correlation between experimental and modeled data for V and C respectively.

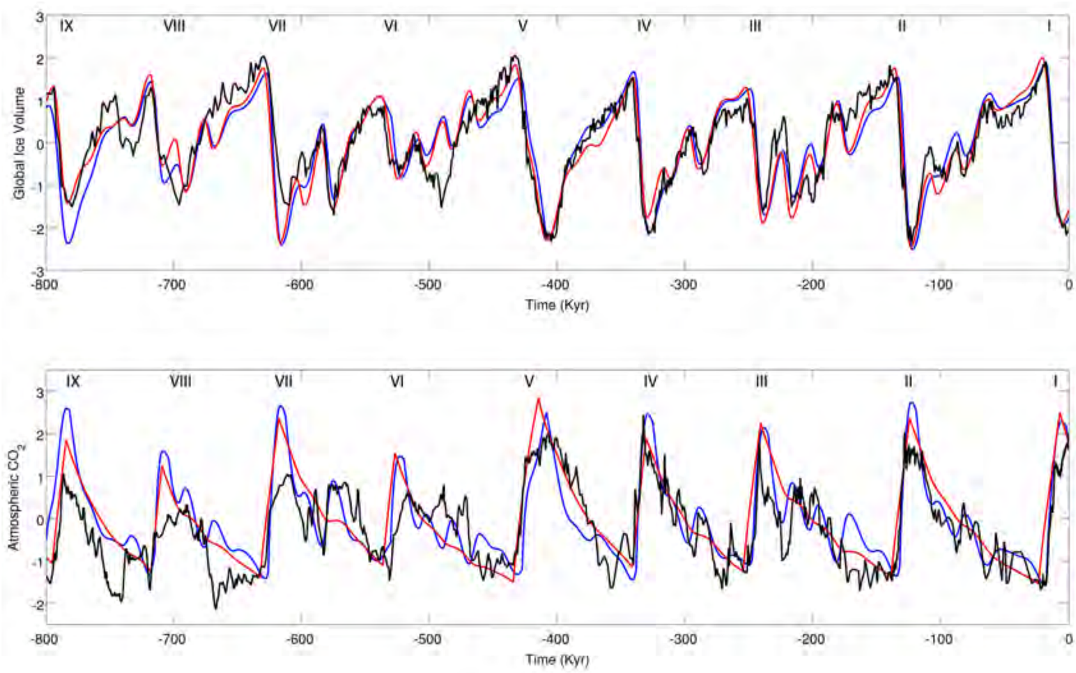

Figure 4.2.2: Comparison between Global ice volume (top) predicted by LMDS (blue), 4τ (red) and $\delta^{18}O$ experimental time-series obtained by *Lisiecki and Raymo* [2005] (black) and CO_2 (bottom) predicted by LMDS (blue), 4τ (red) and experimental time-series obtained by *Luthi et al.* [2008] (black)

terminations IV and VIII are better reproduced than in 4τ (*Figure 4.2.2*) and also timing of termination III, while glacial cycle between 600 and 700 kyr BP remains to be very difficult to simulate. Termination IX, however, became worse especially in the shape.

As can be seen, results are quite encouraging since correctly reproduce major aspects of experimental data with physical variables. A different problem is to decide what confidence can we give to these models with high correlations, given that the record used for the past ice volume suffers probably different biases. Indeed, the record is a stack of $\delta^{18}O$ data from benthic foraminifera, and the ratio $^{18}O/^{16}O$ is known to depend on both the isotopic composition and the temperature of the water in which the foraminifera develops. *Siddall et al.* [2010] found that ice volume becomes increasingly sensitive to temperature change at lower temperatures. *Waelbroeck et al.* [2002] found that the relationship between $\delta^{18}O$ and ice volume is not linear, since $\delta^{18}O$ decreases faster than ice volume increases at the beginning of the last glaciation, and then progressively more slowly until the ice sheets reached their maximum size. This may produce uncertainties larger than 20% for the ice volume estimations in some periods. Thus, the models with the largest correlations between predicted ice volume and $\delta^{18}O$ are not necessarily better than other models with slightly lower correlation, due to the uncertainty in the observational data. This is a complex and important question which would require an additional mathematical analysis that we leave for a future work. Fortunately, there is not such problem for CO_2, which is directly measured in ice cores.

It may appear easy, and not surprising, to get the good fits that have been shown in *Table 3.1* and *4.1* with so many parameters used by the models studied. This is particularly true when experimental data are fitted to generic mathematical functions that are dependent of an arbitrary number of parameters. However, it is not so easy to get the same fit performance with mathematical expressions that imitate geophysical mechanisms, as feedback and pumping rates. An additional outcome from this kind of mechanistic box-models is that they point to specific physical mechanisms that are potentially drivers of the observed changes. Thus, when good fits are obtained with this kind of models, the specific physical mechanisms modeled should be investigated in more detail to confirm that are them (and not an alternative mechanism producing a similar behavior) which are under the observed dynamics.

5 Discussion

The dynamics of overturning, its change and its impact on CO_2 variation during glacial cycles remains controversial (*Sigman et al.* [2010]). However some facts are well established and widely accepted.

First, the deep ocean has northern and southern meridional overturning circulations: NMOC, described as a long loop dominated by North Atlantic Deep Water (NADW), which is relatively poor in dissolved CO_2 due to high photosynthetic consumption; and SMOC, known as a short loop dominated by Antarctic Bottom Water (AABW) which is relatively richer in CO_2 (*Toggweiler et al.* [2006]; *Watson and Garabato* [2006]). Both loops mix in the interior around the Antarctic continent to form Circumpolar Deep Water (CDW), which comes up to the surface along the southern part of the Antarctic Circumpolar Current (ACC). This upwelling is forced mainly by the divergence of Ekman pumping at the surface, centered to lay at approximately 65ºS today (*Toggweiler* [1999]), which is driven by the mid latitude westerlies. Any change in either zonal wind speed or latitude of the westerly wind belt should reduce the SMOC (*Toggweiler et al.* [2006]). However, SMOC intensity seems to be the sum of the mean Ekman transport and opposing mean eddy transport over the ACC. The residual northward transport is strongly controlled by heat gain of the waters when travelling northward (*Karsten and Marshall* [2002]).

Second, during the Last Glacial Maximum (LGM) the deep Atlantic was occupied by a water mass that penetrated northwards from the deep SO (*Shackleton et al.* [2000]; *Negre et al.* [2010]). This requires a transitory imbalance between the convective formation of AABW over the Antarctic shelf and its upwelling in the SMOC and a rate of deep water formation around Antarctica larger than in the Northern Hemisphere. The volume increase of CDW during glaciations should retain a larger fraction of CO_2 out of the atmosphere, because CDW is CO_2 rich (*Skinner* [2009]).

Third, temperatures are close to freezing at all the sites in the glacial ocean, but the deep SO (in sites located within present AABW spreading pathways) was much more saline than today, which implies a density anomaly between the deep SO and surface waters that is three times larger than today (*Adkins et al.* [2002]; *Watson and Garabato* [2006]). This evidence could be a consequence of increased brine rejection in Antarctica in combination with reduced recirculation of AABW to the surface (*Fischer et al.* [2010]).

Four, overturning was nearly, or completely, eliminated during the coldest deglacial interval in the North Atlantic region, beginning with the catastrophic iceberg discharge Heinrich event H1, 17500 yr ago (*McManus et al.* [2004]), in coincidence with the first major step in Antarctic warming (*Barker et al.* [2009]). Some terminations have started in coincidence with Heinrich events.

Both empirical evidence and comparisons of coupled general circulation models for glacial conditions show very little change in the strength of the zonal wind stress on the SO and no clear shift in the location of the westerlies belt (*Fischer et al.* [2010]). However, as suggested by this author, the increase of sea ice coverage could have modulated the annual net heat gain of the SO surface, and the reduced buoyancy gain would have awakened the SMOC, so limiting the upwelling of CO_2-enriched deep water. On the other hand, a change in biological productivity as a result of dust-transported iron fertilization appears as very likely; however, the glacial increase in export production may explain only 10-20 ppmv of the 80-100 ppmv of glacial-interglacial CO_2 difference (*Fischer et al.* [2010]). Finally, there is not evidence of substantial variations in the strength of the Atlantic MOC during the LGM (*Wunsch* [2003]), which was probably only slightly awakened (*Lynch-Stieglitz et al.* [2007]). However, the influence of sea ice extent on SMOC intensity, through its control on the residual circulation, seems to be much more efficient according to *Fischer et al.* [2010]. This effect would act in the same direction as the capping effect that winter ice extent is supposed to have on deep-water out gassing of CO_2 (*Stephens and Keeling* [2000]).

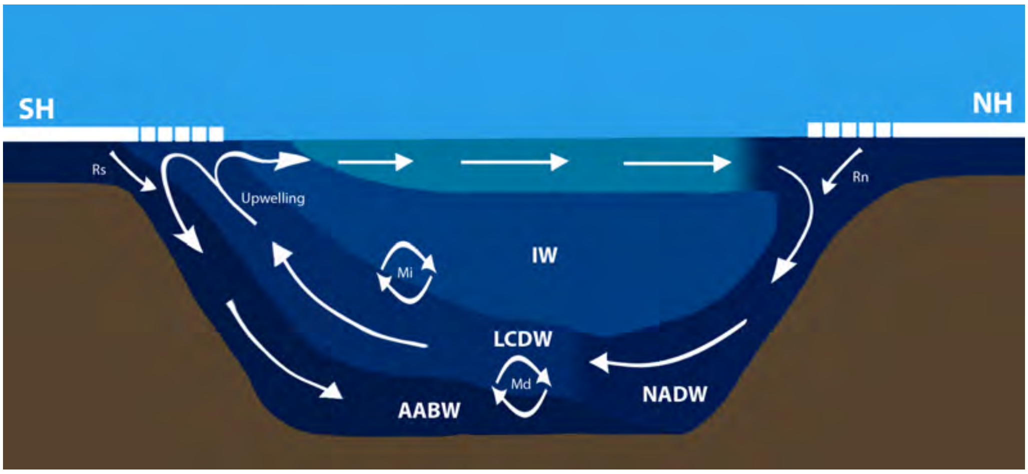

Figure 5.0.1: Schematic representation of the main mechanisms controlling the deep ocean emission of CO_2.

Figure 5.0.1 is a schematic diagram illustrating some of the mechanisms discussed. M_d is the deep diapycnal mixing of water masses around Antarctica which causes Low Circumpolar Deep Water (LCDW) to be richer or poorer in AABW. M_i symbolizes the mixing between LCDW (a mix of NADW and AABW) and the intermediate waters above (IW), and R_n and R_s are the rates of formation of dense water at northern and southern high latitudes, respectively.

Mixing rates M_d and M_i are driven by turbulence. There are reasons to believe that mixing rates may decrease as density differences increase (*Watson and Garabato* [2006]) if we use an internal wave parametrization for the vertical mixing coefficient suggested by *Gargett* [1984]. Therefore, if the density difference between AABW and NADW is small, the blending process M_d of the two water masses is more efficient and a larger fraction of the AABW wells up with the mixed LCDW into the two loops of the MOC (NMOC and SMOC). Overturning should also increase in this situation, because one part of the MOC is driven by turbulence-driven diapycnal mixing M_d and M_i, albeit to a limited degree, because an important part of the upwelling is driven by the isopycnal Ekman pumping (*Kuhlbrodt et al.* [2007]).

In LMDS, F has a dependence on local variables through A and C and also a direct dependence on V, which can be explained by the *Gildor and Tziperman* [2001] mechanism of teleconnection between northern temperature and southern sea ice formation, via advection of NADW.

The A variable is crucial in the models we are studying, and it should be interpreted as SO sea ice being in agreement with *Fischer et al.* [2010] synthesis. The efficiency in the formation of deep water F is another crucial variable of the models, which supports the probable importance of density difference between AABW and NADW in controlling the upwelling of CO_2. This may take place through variation of the mixing rate M_i in the *Gildor and Tziperman* [2001] interpretation or M_d in *Paillard and Parrenin* [2004]. In our interpretation, both mechanisms may be acting in the same direction, generating a lower M_i and M_d during glacial times. The enhanced A during these periods also have an influence through its control on upwelling intensity. These three mechanisms, which act always in the same direction, may explain the differences between glacial and interglacial periods.

One conclusion of this study is that I_{60} is not a good proxy for Southern Hemisphere temperature. LMDS suggests that the formation of the densest waters is strongly controlled by the sea ice extent A, and that this ice extent is very dependent on the temperature of the water upwelled in the SO, through C (as suggested for *Paillard and Parrenin* [2004]). But it could be coherent with an alternative explanation: A is very dependent on SO climate, which co-varies with I_{65} and, thus, also to some extent with V (conclusion arised from *Gildor and Tziperman* [2001]). Therefore, both mechanisms, Tziperman's teleconnection and Paillard's deep stratification, could be plausibly acting in parallel, in the same direction, according with the good performance obtained with our LMDS model.

But which of these suggested mechanisms is the one that triggers the glacial-interglacial transition? In *Gildor and Tziperman* [2001] model the ultimate trigger is northern ice-sheet instability due to reduced evaporation in the presence of extensive sea-ice during the glacial paroxysm. This instability would produce a heating pulse that would be transmitted to the SO via NADW teleconnection. However, this sequence of events does not seem to be in agreement with some observations (*Paillard* [1998]). The explanation of *Paillard and Parrenin* [2004] is different: after the glacial paroxysm, the rate of formation of the densest waters becomes zero or negligible, due to the disappearance of active polinyas in the thick ice sheet extending beyond the Antarctic shelf. A plausible effect of it is that density difference between AABW and NADW decreases by turbulent mixing M_d. The effect of a lower density difference is to increase M_d, which accelerates density mixing through a positive feedback. After a few thousand years, LCDW becomes richer in AABW and CO_2

and so does the LCDW upwelling, which produces the CO_2 pulse that is needed to trigger deglaciation, especially if the glacial paroxysm coincides with a sudden heating of the SO, due to a Heinrich event, to astronomical forcing or to stochastic occurrence of a set of warm summers in the SO. A sudden heating of the SO, we conjecture, should produce a quick release of CO_2 to atmosphere due to decrease of solubility of the (CO_2 rich) SO surface waters.

If Antarctic climate is in phase with northern climate (*Huybers and Denton* [2008]), the observed dependence of F in our LMDS model on V and A would be compatible with both mechanisms, agreeing with some recent works (*Laepple et al.* [2011]) and offering an alternative path to be more carefully explored. Even so, more research about the crucial role that SO temperature plays in F variations is needed to decide if the oceanic pulse triggered should be interpreted as an intensification of M_d, of M_i, of both of them, or if it is related mainly to the control of sea ice extent on SO upwelling.

Acknowledgements

This work is a contribution to the project MOC-2 funded by the Spanish R+D Plan 2008-2011. I would like to thank Antonio García-Olivares and Josep Lluís Pelegrí for their great support, help, and confidence; as well to Eva Calvo and Carles Pelejero for their interesting suggestions and help with experimental data; and to Didier Paillard, for his useful comments. I wish to dedicate this work to my family, for their unconditional support and patience.

Bibliography

Adkins, J. F., K. McIntyre, and D. P. Schrag, The salinity, temperature, and δ^{18}o of the glacial deep ocean, *Science*, *298*(5599), 1769–1773, 2002.

Archer, D., and E. Maier-Reimer, Effect of deep-sea sedimentary calcite preservation on atmospheric co$_2$ concentration, *Nature*, *367*(6460), 260–263, 1994.

Archer, D., A. Winguth, D. Lea, and N. Mahowald, What caused the glacial/interglacial atmospheric pco$_2$ cycles?, *Rev. Geophys.*, *38*(2), 159–189, 2000.

Archer, D., et al., Atmospheric lifetime of fossil fuel carbon dioxide, *Annual Review of Earth and Planetary Sciences*, *37*(1), 117–134, 2009.

Bard, E., B. Hamelin, M. Arnold, L. Montaggioni, G. Cabioch, G. Faure, and F. Rougerie, Deglacial sea-level record from tahiti corals and the timing of global meltwater discharge, *Nature*, *382*(6588), 241–244, 1996.

Barker, S., P. Diz, M. J. Vautravers, J. Pike, G. Knorr, I. R. Hall, and W. S. Broecker, Interhemispheric atlantic seesaw response during the last deglaciation, *Nature*, *457*(7233), 1097–1102, 2009.

Berger, A., *A simple algorithm to compute long term variations of daily or monthly insolation.*, vol. 18, 18 ed., Contribution de l'Institut d'Astronomie et de Geophysique, Universite Catholique de Louvain. Louvain-la-Neuve. Belgium, 1978a.

Berger, A., Long term variations of daily insolation and quaternary climatic changes, *Journal of the Atmospheric Sciences*, *35(12)*, 2362–2367, 1978b.

Broecker, W. S., Glacial to interglacial changes in ocean chemistry, *Progress In Oceanography*, *11*(2), 151 – 197, 1982.

Charbonneau, P., *An introduction ot genetic algorithms for numerical optimization*, High Altitude Observatory, National Center for Atmospheric Research. Boulder, Colorado., 2002.

Curry, W. B., and D. W. Oppo, Glacial water mass geometry and the distribution of δ^{13}c of σco$_2$ in the western atlantic ocean, *Paleoceanography*, *20*(1), PA1017–, 2005.

Fischer, H., et al., The role of southern ocean processes in orbital and millennial co$_2$ variations - a synthesis, *Quaternary Science Reviews*, *29*(1-2), 193 – 205, 2010.

Ganopolski, A., R. Calov, and M. Claussen, Simulation of the last glacial cycle with a coupled climate ice-sheet model of intermediate complexity, *Climate of the Past*, *6*(2), 229–244, 2010.

García-Olivares, A., and C. Herrero, Fitting the last pleistocene delta o-18 and co_2 time-series with simple box models, *Scientia Marina*, 2011.

Gargett, A., Vertical eddy diffusivity in the ocean interior, *Journal of Marine Research*, *42*(2), 359–393, 1984.

Gildor, H., and E. Tziperman, Physical mechanisms behind biogeochemical glacial-interglacial co_2 variations, *Geophys. Res. Lett.*, *28*(12), 2421–2424, 2001.

Hays, J. D., J. Imbrie, and N. J. Shackleton, Variations in the earth's orbit: Pacemaker of the ice ages, *Science*, *194*(4270), 1121–1132, 1976.

Herrero, C., A. García-Olivares, and J. L. Pelegrí, El ciclo glacial-interglacial. análisis y mejora del modelo de paillard, in *I Encuentro de la Oceanografía Física Española (EOF). Barcelona, Spain. Poster*, 2010.

Herrero, C., A. García-Olivares, and J. L. Pelegrí, Simulations of glacial/interglacial cycles with simple box-models. key triggers for deglaciations, in *Goldschmidt Conference. Prague, Czech Republic. Poster*, 2011.

Huybers, P., and G. Denton, Antarctic temperature at orbital timescales controlled by local summer duration, *Nature Geosci*, *1*(11), 787–792, 2008.

Karsten, R. H., and J. Marshall, Constructing the residual circulation of the acc from observations, *J. Phys. Oceanogr.*, *32*(12), 3315–3327, 2002.

Keeling, R. F., and B. B. Stephens, Antarctic sea ice and the control of pleistocene climate instability, *Paleoceanography*, *16*(1), 112–131, 2001.

Knox, F., and M. B. McElroy, Changes in atmospheric co_2: Influence of the marine biota at high latitude, *J. Geophys. Res.*, *89*(D3), 4629–4637, 1984.

Kohfeld, K. E., C. L. Quere, S. P. Harrison, and R. F. Anderson, Role of marine biology in glacial-interglacial co_2 cycles, *Science*, *308*(5718), 74–78, 2005.

Kuhlbrodt, T., A. Griesel, M. Montoya, A. Levermann, M. Hofmann, and S. Rahmstorf, On the driving processes of the atlantic meridional overturning circulation, *Rev. Geophys.*, *45*(2), RG2001–, 2007.

Laepple, T., M. Werner, and G. Lohmann, Synchronicity of antarctic temperatures and local solar insolation on orbital timescales, *Nature*, *471*(7336), 91–94, 2011.

Lisiecki, L. E., and M. E. Raymo, A pliocene-pleistocene stack of 57 globally distributed benthic delta o-18 records, *Paleoceanography*, *20*(1), PA1003–, 2005.

Luthi, D., et al., High-resolution carbon dioxide concentration record 650,000-800,000 years before present, *Nature*, *453*(7193), 379–382, 2008.

Lynch-Stieglitz, J., et al., Atlantic meridional overturning circulation during the last glacial maximum, *Science*, *316*(5821), 66–69, 2007.

McManus, J. F., R. Francois, J.-M. Gherardi, L. D. Keigwin, and S. Brown-Leger, Collapse and rapid resumption of atlantic meridional circulation linked to deglacial climate changes, *Nature*, *428*(6985), 834–837, 2004.

Monnin, E., A. Indermuhle, A. Dallenbach, J. Fluckiger, S. Bernhard, T. F. Stocker, D. Raynaud, and J.-M. Barnola, Atmospheric co_2 concentrations over the last glacial termination, *Science*, *291*, 112–114, 2001.

Negre, C., R. Zahn, A. L. Thomas, P. Masque, G. M. Henderson, G. Martinez-Mendez, I. R. Hall, and J. L. Mas, Reversed flow of atlantic deep water during the last glacial maximum, *Nature*, *468*(7320), 84–88, 2010.

Olivella, R., Modelizacion de la respuesta glacial-interglacial del co_2 atmosferico mediante un modelo fisiologico oceanico, Master's thesis, Universidad de Las Palmas de Gran Canaria, 2009.

Paillard, D., The timing of pleistocene glaciations from a simple multiple-state climate model, *Nature*, *391*(6665), 378–381, 1998.

Paillard, D., Climate and the orbital parameters of the earth, *Comptes Rendus Geoscience*, *342*(4-5), 273 – 285, 2010.

Paillard, D., and F. Parrenin, The antarctic ice sheet and the triggering of deglaciations, *Earth and Planetary Science Letters*, *227*(3-4), 263 – 271, 2004.

Parrenin, F., and D. Paillard, Amplitude and phase of glacial cycles from a conceptual model, *Earth and Planetary Science Letters*, *214*(1-2), 243 – 250, 2003.

Pelegrí, J. L., A pysiological approach to oceanic processes and glacial-interglacial changes in atmospheric co_2, *Scientia Marina*, *72*, 185–202, 2008.

Pelegrí, J. L., R. Olivella, and A. García-Olivares, A simple metabolic model of glacial-interglacial energy supply to the upper ocean, *Earth System Dynamics Discussions*, *2*(1), 271–313, 2011.

Pepin, L., D. Raynaud, J. M. Barnola, and M. F. Loutre, Hemispheric roles of climate forcings during glacial-interglacial transitions as deduced from the vostok record and lln-2d model experiments, *Journal of Geophysical Reviews*, *106*, 31,885–31,892, 2001.

Petit, J. R., et al., Climate and atmospheric history of the past 420000 years from the vostok ice core antarctica., *Nature*, *399*, 429–436, 1999.

Shackleton, N. J., M. A. Hall, and E. Vincent, Phase relationships between millennial-scale events 64,000-24,000 years ago, *Paleoceanography*, *15*(6), 565–569, 2000.

Siddall, M., B. Honisch, C. Waelbroeck, and P. Huybers, Changes in deep pacific temperature during the mid-pleistocene transition and quaternary, *Quaternary Science Reviews*, *29*(1-2), 170 – 181, 2010.

Siegenthaler, U., et al., Stable carbon cycle-climate relationship during the late pleistocene., *Science*, *310*, 1313–1317, 2005.

Sigman, D. M., and E. A. Boyle, Glacial/interglacial variations in atmospheric carbon dioxide, *Nature*, *407*(6806), 859–869, 2000.

Sigman, D. M., M. P. Hain, and G. H. Haug, The polar ocean and glacial cycles in atmospheric co2 concentration, *Nature*, *466*(7302), 47–55, 2010.

Skinner, L. C., Glacial-interglacial atmospheric co_2 change: a possible "standing volume" effect on deep-ocean carbon sequestration, *Climate of the Past*, *5*(3), 537–550, 2009.

Stephens, B. B., and R. F. Keeling, The influence of antarctic sea ice on glacial-interglacial co_2 variations, *Nature*, *404*(6774), 171–174, 2000.

Toggweiler, J. R., Variation of atmospheric co_2 by ventilation of the ocean's deepest water, *Paleoceanography*, *14*(5), 571–588, 1999.

Toggweiler, J. R., and J. L. Sarmiento, Glacial to interglacial changes in atmospheric carbon dioxide: The critical role of ocean surface water in high latitudes. in the carbon cycle and atmospheric co_2: Natural variations archean to present, *Geophys. Monograph, American Geophysica Union*, *32*, 163 – 184, 1985.

Toggweiler, J. R., J. L. Russell, and S. R. Carson, Midlatitude westerlies, atmospheric co_2, and climate change during the ice ages, *Paleoceanography*, *21*(2), PA2005–, 2006.

Waelbroeck, C., L. Labeyrie, E. Michel, J. Duplessy, J. McManus, K. Lambeck, E. Balbon, and M. Labracherie, Sea-level and deep water temperature changes derived from benthic foraminifera isotopic records, *Quaternary Science Reviews*, *21*(1-3), 295 – 305, 2002.

Watson, A., and A. C. N. Garabato, The role of southern ocean mixing and upwelling in glacial-interglacial atmospheric co_2 change, *Tellus B*, *58*(1), 73 – 87, 2006.

Wunsch, C., Determining paleoceanographic circulations, with emphasis on the last glacial maximum, *Quaternary Science Reviews*, *22*(2-4), 371 – 385, 2003.

Corrigendum

Msc Thesis. Universidad de Las Palmas de Gran Canaria

Simulations of glacial/interglacial cycles with simple box-models. The ocean CO_2 source during deglaciations

Carmen Herrero i Navarro

January 24, 2012

- In Figure 2.1.1 the y axes *Northern Hemisphere Summer Insolation (W/m²)* and *Late Austral Summer Insolation (W/m²)* shall be replaced by *Northern Hemisphere Summer Insolation* and *Late Austral Summer Insolation*.

- In Equations 3.1.5, 3.2.5, 4.1.5 and 4.2.5 the parameter $\gamma H(F)$ shall be replaced by $\gamma H(-F)$.